Title:

Deformation structures associated with the Tazo landslide (La Gomera, Canary Islands).

Authors:

Ramón Casillas[1], Carlos Fernández[2], Juan Ramón Colmenero[3], Julio de la Nuez[1], Encarnación García-Navarro[2] and M. Candelaria Martín[1]

1: Dpto. de Edafología y Geología. Fac. de Biología. C/Astrofísico Sánchez s/n. Universidad de La Laguna. 38206. La Laguna. Santa Cruz de Tenerife. Phone: 34-922-318373. Fax: 34-922-318311. rcasilla@ull.es.

2: Dpto. de Geodinámica y Paleontología, Fac. de Cc. Experimentales, Universidad de Huelva, 21071-Huelva.

3: Dpto Geología, Facultad de Ciencias, Univ. de Salamanca, Plaza de la Merced s/n 37008 Salamanca.

Abstract:

Deformation structures below the basal plane of gravitational slides can provide useful information about the state of stress undergone by rocks prior to the sliding process and about the triggering forces acting at each particular sliding event. In the present work

we conducted a structural analysis of the rocks below the surface of the gravitational lide of Tazo (La Gomera, Canary Islands) and determined the epigenetic processes involved in the filling of the amphitheatre. We also inferred the possible triggering phenomena related to the Tazo landslide. The rocks located below the surface of the gravitational slide of Tazo -i.e., the basaltic lava flows, sills and dikes of the Lower Old Edifice and the submarine volcanic rocks, gabbros, pyroxenites and dikes of the Basal Complex of La Gomera- are strongly deformed close to this sliding surface. The lava flows and dikes of the Lower Old Edifice are folded, with fault breccias and gouges, and locally foliated, defining the sliding surface. The dikes of the Basal Complex are also folded, and the gabbros and pyroxenites are affected by a large number of small faults. In the Basal Complex, the sliding surface is defined by a foliated granular gouge. In the damage zone, the Basal Complex rocks show an incipient fracture cleavage. The sliding amphitheatre has been filled by the debris avalanche or cohesive debris flow generated within the slide, as well as by later debris flows, hyperconcentrated flows, sheet flows, and by interspersed lava flows from the Upper Old Edifice. We suggest here that the collapse of the north-western flank of the Lower Old Edifice at Tazo could in part have been triggered by continuous magma injection, associated with the emplacement of dikes in a rift zone with an ENE-WSW direction, enhanced by the mechanical weakness of the Basal Complex unit, which was affected by hydrothermal metamorphism under greenschist facies conditions and by the displacement along the Montaña de Alcalá and Guillama normal faults, which are deeply entrenched in the altered rocks of the Basal Complex.

Key words:

La Gomera, Canary Islands, Tazo landslide, deformation, debris avalanche, debris flow.

INTRODUCTION.

Gravitational landslides on the flanks of large volcanic edifices are one of the most spectacular and catastrophic phenomena that occur at volcanic oceanic islands during their evolution. Many studies have been conducted to analyze the geometry of the scars formed by these landslides, the resulting deposits, and the possible causes of such events. Nevertheless, few studies have analyzed the deformation suffered by the rocks located just below the main slide plane (Schneider and Fisher 1998; Bachèlery et al. 2003) or the epigenetic/sedimentary processes involved in the filling of landslide amphitheatres. Active volcanoes are unlikely to be suitable for such studies, because even when they are temporarily exposed in fault scarps the fault rocks themselves are likely to be rapidly buried by lavas, pyroclastic deposits, and volcaniclastic sediments covering the scarps. A more profitable approach may be to study ancient exhumed structures.

In some slide structures on ocean islands, the rocks underneath the slip plane show features indicative of a strong, mostly brittle deformation, such as at La Palma (Roa 2003), with numerous faults and associated secondary fractures, folds, tilted dikes, and shearing of the dike margins, such as the Taganana and Teno Alto slides in Tenerife (Walter et al. 2005; Walter and Schmincke 2002). The shearing of rocks below the sliding surfaces suggests that creep was active prior to the slide event, causing intense deformation of the rocks involved. Also remarkable is the presence of strong striations under the Toreva or mega-blocks produced by the sliding of these blocks above the

98 slide plane, such as at La Palma (Roa 2003) and Gran Canaria (Mehl and Schmincke
99 1999).
100
101 Deformation studies of rocks below the slide plane can provide useful insights into
102 the stress conditions of rocks prior to the slide process. Such research can help to reveal
103 the ultimate causes of each particular slide event. In this sense, La Gomera island
104 (Canary Islands) provides an interesting opportunity for structural analysis, since the
105 rocks appearing below the slide plane that affected the north-western sector of the
106 Lower Old Edifice -termed the Tazo landslide (Ancochea et al. 2006)- exhibit
107 associated deformation structures. Currently, little is known about the volcanic and
108 sedimentary processes involved in the filling of the scars formed by gravitational flank
109 slides. There appears to be some confusion regarding discrimination between the
110 deposits directly formed by flank sliding (essentially "debris avalanche") and the
111 sediments related to the filling of the slide scars, deposited by gravity flows well after
112 the sliding process (essentially "debris flow") or by running water (essentially
113 hyperconcentrated flows and sheetfloods). The Tazo flank landslide on La Gomera led
114 to the formation of a large landslide amphitheatre that was later filled with sedimentary
115 deposits (polygenetic agglomerates, Cendrero 1971) and numerous basaltic lava flows.
116 The oldest of these basaltic flows are interbedded with sedimentary deposits and form
117 part of the Upper Old Edifice (Ancochea et al. 2006).
118
119 The main aim of this work is to describe the deformation structures that appear
120 below the basal plane of the Tazo landslide, and to investigate the deformation
121 mechanisms involved in the slide. Another objective is to describe the amphitheatre
122 deposits in order to explain the volcanic and sedimentary processes involved in the

filling of this amphitheatre. A final aim is to deduce the causes of this gravitational slide in light of these data.

GEOLOGICAL SETTING.

The oldest outcropping rocks of La Gomera (Fig. 1 and Fig. 2) are the marine sediments, submarine volcanic rocks, plutonic rocks and dikes forming the Basal Complex (Bravo 1964; Cendrero 1971). The submarine volcanic rocks outcrop in the north-western sector of the island and are constituted by basaltic pillow lavas, peperites, breccias, volcanic sandstones and siltstones, and trachytic breccias of unknown age (Cendrero 1971). Sub-vertical layers of marine sediments of unknown age (sandstones, limestones, cherts and carbonate layers) are related to these submarine rocks (Cendrero 1971). A suite of plutonic rock bodies, dated at between 19.8 and 7.5 Ma, appears in the Basal Complex (Abdel-Monem et al. 1971; Cantagrel et al. 1984; Herrera et al. 2008). Taking into account the spatial relationships of the plutonic rocks and the effects of contact metamorphism, they can be grouped within three plutonic events of different ages (Cendrero 1971; Démeny et al. 2010), a) hornblende pyroxenites (with kaersutite as the dominant amphibole), hornblendites (with kaersutite as the dominant amphibole), and amphibole gabbros (P1); b) wehrlites, clinopyroxenites, olivine gabbros and gabbros (P2) and c) alkaline gabbros, monzodiorites and syenites (P3, Tamargada Complex). An important dike swarm intrudes these sedimentary, volcanic and plutonic rocks (Cendrero 1971). This dike swarm is characterized by a high dike density and compositional variety, in spite of its dominant N70º-80º strike. All the rocks of the Basal Complex are strongly faulted (Cendrero 1971) and have been affected by a strong hydrothermal metamorphism in greenschist conditions that led to the formation of

148 hornblende, actinolite, epidote, albite and chlorite.

149

150 La Gomera island began to emerge around 10.5 Ma ago with the formation of
151 the Old Edifice (formed between 10.5 and 6.4 Ma), with shallow submarine rocks at the
152 base (Ancochea et al. 2006). Two stages of growth of the Old Edifice have been
153 distinguished. In the first stage, a large basaltic shield edifice was formed (Lower Old
154 Edifice), with a diameter of 22 km (Ancochea et al. 2006). This edifice underwent
155 several flank slide events (e.g. Tazo and San Marcos) that dismantled a large portion of
156 its northern sector (Paris et al. 2005; Ancochea et al. 2006). In the second stage of
157 growth (Upper Old Edifice), the activity migrated to the south and a wide composite
158 volcano with a diameter of 25 km was developed, covering the rocks of the Lower Old
159 Edifice. Finally, a young volcanic edifice grew (Young Shield Edifice) between 5.7 and
160 4 Ma ago (Ancochea et al. 2006). The lava flows of this edifice covered the central and
161 southern parts of the island completely, filling up deep valleys in the north.

162

163 **THE TAZO LANDSLIDE.**

164

165 **General description**

166

167 The Tazo landslide (Figs. 1, 2 and 3A) occurs in the north-western sector of La
168 Gomera and it affected the north-western flank of the Lower Old Edifice. The age of the
169 sliding has been dated at about 9.4 Ma (Ancochea et al. 2006). The flank landslide left a
170 large scar that was filled up with debris avalanche, debris flow, hyperconcentrated flow,
171 and sheetflood deposits corresponding to the polygenetic agglomerates of Cendrero
172 (1971). At the same time, volcanic activity was reinitiated, giving rise to numerous

173 basaltic flows that formed the Upper Old Edifice (Ancochea et al. 2006). The oldest of
174 these basaltic flows are interbedded with the sedimentary deposits filling the slide scar
175 (Herrera 2008).
176
177 The basal plane of the Tazo slide outcrops extensively in the Tazo-Alojera-
178 Argüamul-Guillama sector. Towards the Northeast (Argüamul-Guillama) and to the
179 South (Tazo), the rocks of the Basal Complex outcrop below the plane. These are
180 submarine volcanic rocks, gabbros and pyroxenites, intensely intruded by dikes of
181 varying composition. Northwestwards (Alojera-Bejira), the basaltic flows of the Lower
182 Old Edifice appear below the sliding surface, dipping towards the northwest, and they
183 are intruded by sills and vertical dikes of the same composition. The slip plane is
184 truncated by the present-day coastline (Fig. 2) and has been eroded by wave action and
185 by the frequent Quaternary coastal slides that have occurred in this sector, such as that
186 of Arguamul (Paris et al. 2005). Inland, the slip plane is overlain by the horizontal lava
187 flows of the Young Shield Edifice (Fig. 3A). The highest altitude of the sliding surface
188 outcrops is 830 meters, at Epina (Fig. 3A).
189
190 **Structures associated with the Tazo landslide**
191
192 On the coast, between La Punta del Peligro and La Baja del Picacho, large cliffs
193 expose a major contact, defined by a continuous and regular surface dipping 20º
194 towards the north (Point 1 in Fig. 2, Fig. 3B). This major contact will be referred to as
195 “contact surface” throughout this section of the structural description. A volcanic
196 breccia can be observed above the contact surface, and curved lava flows, sills and dikes
197 of the Lower Old Edifice lie below it. Trachyphonolitic dikes of the radial dike complex

198 (Ancochea et al. 2006) associated with the Vallehermoso felsic rocks (Fig. 1) and some
199 undeformed basaltic dikes cross-cut the contact plane, which has been displaced by
200 normal faults dipping towards the southwest.
201
202 The same contact surface is visible near the small village of Cubaba (Point 2 in
203 Fig. 2), where it is possible to observe the deformation that has affected the dikes and
204 lava flows of the Lower Old Edifice in detail (Fig. 4). Around 100 m below the contact
205 surface, the Lower Old Edifice is composed of 1-m-thick flows of basaltic pahoehoe
206 lava. Thin sills and E-W oriented, subvertical, less than 1-m-thick basaltic dikes, with
207 an average spacing of 10 to 15 m, have intruded the lava flows. These rocks do not
208 show evidence of deformation. At around 15 m below the contact surface, the lava
209 flows and sills are cross-cut by subvertical cracks infilled by highly cemented breccias
210 formed by subangular and heterogranular fragments of lava flows and basaltic dikes,
211 with diameters of up to 5 cm (Fig. 4A). These infilled cracks are typically between 0.5
212 and 5 m thick and are WNW-ESE oriented. The widest ones have a wedged geometry
213 and are infilled by a breccia similar to the one located above the major contact surface.
214 At around 10 m below the contact surface the basaltic flows and sills are thinned and
215 stretched and appear completely broken and brecciated, although their edges are still
216 recognizable. They are overturned and form folds (Figs. 4B and Fig. 5A, B). The spatial
217 orientation of the sill walls and lithological layering (S_0) separating the distinct lava
218 flows has been measured in the field and is projected (great circles) in Fig. 5A. If
219 measurements were made without error and the fold was perfectly cylindrical all the
220 great circles would pass through the same axis, which coincides with the fold axis
221 (Ramsay and Huber 1987). However, these conditions are rarely, if ever, met (see Fig.
222 5A). Fold axes can be determined with maximum accuracy by finding a best-fit great

223 circle for the poles of the measured data, the perpendicular to this great circle lying
224 parallel to the fold axis (Ramsay and Huber 1987). A standard statistical procedure to
225 determine the best-fit great circle and its normal line is to compute the eigenvectors of
226 the matrix that expresses the moment of inertia of the poles to the measured data in a
227 given direction (Mardia 1972). The eigenvector associated with the maximum moment
228 of inertia represents the line most normal to all the measured poles as possible, thus
229 representing the statistically determined fold axis. A confidence level can be assigned to
230 the results of this procedure. The statistically determined axes of the folds measured at
231 Point 2, for both S_o and the sill walls, plunge slightly to the north (Fig. 5A) and are sub-
232 parallel to the main contact surface. The fold geometry can best be described as a
233 progressive rotation of lava flows and sills from a regional, northwest-dipping attitude
234 towards a position parallel to the contact surface (large arrow in Fig. 5A).
235
236 Around 4 m below the contact surface, the lava flows and sills are very
237 deformed. It is possible to observe individual sills and lava flows that have become
238 progressively reoriented, stretched and brecciated while approaching the contact
239 surface, forming a fault breccia (Fig. 4B) composed of very angular fragments of up to
240 2-5 cm in diameter without matrix. There are cracked grains (jigsaw fit); –i.e. angular
241 fragments that have been fractured without much displacement, such that the original
242 spatial relationships of the fragments can still be recognized. The fragments, which are
243 very angular, do not appear to have been rotated. Here the sub-vertical dikes show a
244 curved geometry, reaching a sub-horizontal orientation a few meters below the slide
245 plane. Moreover, they display a fragmented pattern similar to that of the lavas and sills.
246 At only 1 m below the contact surface, the dikes and the lava flows are crushed, and the
247 fragments of each unit define thinned and stretched bands, following planes that are

parallel to the slide surface and forming foliated breccias (Fig. 4C). Closer to the contact surface, the stretched bands give rise to a foliated granular gouge. In this zone, it is frequently possible to recognize the different lava flows and dikes, in spite of the intense fracturing, with fragments of up to 10-15 cm included in a fine-grained cataclastic matrix. The fragments may have undergone a small rotation. Above the contact plane, a poorly sorted, unstratified and structureless**,** highly heterogranular and heterolithologic breccia occurs. It contains subangular fragments of lava flows and dikes of up to 1 m in maximum diameter (Fig. 4D). The matrix of this breccia is composed of angular fragments of volcanic rocks, dikes, and plutonic rocks, with highly heterometric grain-size populations, ranging from fine gravel to clay.

In the La Barca Valley (Point 3 in Fig. 2), the foliated-to-granular gouge located immediately below the contact plane often displays fragment mixing, abrupt changes in unit thickness, folding, flow structures, and other signs of mesoscopic ductility (Miller 1996). Microscopically, this gouge contains survivor grains (between 0.2 and 5 mm) composed of basaltic fragments, typically rounded to sub-rounded and showing little evidence of fracturing, crystal-plastic deformation, dissolution, or mineral growth. The survivor grains are floating in a foliated or banded matrix composed of clay minerals and/or extremely fine grained (< 0.01 mm) remnants of the parent rock, plagioclase, and pyroxene crystals.

Near Tazo (Point 4 in Fig. 2), dike-injected gabbros and pyroxenites of the Basal Complex are present below the contact surface. This surface trends NNW-SSE to NE-SW and dips slightly to the West (Fig. 5C). As at Point 1, the plutonic rocks and dikes are strongly deformed around 20 m below the contact surface. These deformed rocks

273 display numerous closely-spaced small faults that define a fracture cleavage. The
274 breccia located in the hanging wall of the contact surface is also faulted near its basal
275 contact. The slickenside features of these faults are indicative of the slip motion along
276 the main contact surface. These faults were analyzed with the kinematic PT method of
277 Marrett and Allmendinger (1990) to obtain the orientation of the principal deformation
278 axes (the results of the PT method for the different measurement points are shown in
279 Supplementary Material). The faults measured are predominantly normal and hence the
280 maximum shortening (P axis) is almost vertical. The principal extension (T axis) is sub-
281 horizontal and trends N43ºE (Fig. 5C). In the most severely deformed zone,
282 immediately below the contact surface, a foliated granular gouge with an average
283 thickness of about 20 cm and very angular fragments can also be observed (Fig. 6A).
284 Beneath this gouge layer, there is a fault breccia with angular fragments of dikes and
285 plutonic rocks showing polished and striated facets. In the foliated granular gouge, the
286 larger fragments (up to 5 cm) seem to have been rotated and are considered survivor
287 grains (Cladouhos 1999). Sometimes the foliated granular gouge displays evidence of
288 mobilization because it has infilled small cracks that cut across the contact surface and
289 the overlying deposits of the volcanic breccia (Fig. 6B). Above the contact surface, a
290 volcanic breccia showing sharp contacts can be observed, whose sedimentary features
291 are similar to those of the volcanic breccia overlying the contact surface at Point 2. The
292 contact surface is frequently affected by later E-W- to NE-SW-trending normal and
293 reverse faults (Fig. 5C), which points to late NW-SE directed displacements.
294
295 Near Tazo (Point 5 in Fig. 2), the contact surface is E-W-trending and dips
296 slightly to the North (Figs. 6C and Fig. 7A). Above the contact surface there is a
297 volcanic breccia overlying an ultrafine-grained gouge (particles < 62.5 μm) composed

298 of angular fragments of volcanic and plutonic rocks. This gouge layer (Fig. 7A), in
299 which ENE-WSW-trending striae can be observed, shows an average thickness of about
300 2 cm. The striae and associated steps indicate the direction of motion along the contact
301 surface (top towards the ENE, small arrows in Fig. 7A). The PT method reveals a
302 N56ºE-trending principal extension for these predominantly normal faults (large open
303 arrows in Fig. 7A). This estimated direction of extension is compatible with the small-
304 scale kinematic indicators along the contact surface described above. Beneath the
305 contact surface, the dikes intruding the gabbros are folded (Fig. 6C). The statistical fold
306 axis plunges 14º towards N75ºE (Fig. 7A) and is almost parallel to the extension and
307 sliding direction along the main contact surface. Far away from the major contact, the
308 dikes dip at high angles to the SE and show a curved geometry below the contact
309 surface, tending to become parallel with that surface (large curved arrow in Fig. 7A).
310
311 On the road from Tazo to Montaña de Alcalá (Point 6 in Fig. 2), the contact
312 surface shows steep dips to the WNW (Fig. 7B). The faults located in the close vicinity
313 of this contact are sub-parallel to it and their slickenside features show that they are
314 normal faults with hanging wall blocks exhibiting westward, down-thrown motions (old
315 striae in Fig. 7B). However, in some cases it is possible to observe a second set of striae
316 that partially erases the previous set and indicates a late strike-slip reactivation of the
317 contact surface. The layer of ultrafine-grained gouge located at the contact surface can
318 be seen in Fig. 6D. A fault measurement station was set up at the breccias located above
319 the contact surface at this point. The results of the PT method show that the principal
320 direction of extension is sub-horizontal and trends N21ºE; i.e. intermediate between the
321 old and new kinematic indicators observed along the contact surface (Fig. 7B, large
322 white arrows).

323

324 **Sedimentological features of the rocks infilling the flank-collapse amphitheatre**

325

326 The epiclastic deposits that partially infill the Tazo landslide depression outcrop
327 markedly at the Santa Catalina beach and the adjacent Punta del Peligro cliffs. As in
328 other giant landslides found in the Canary Islands, the infilling sequence of the Tazo
329 slide scarp involved two successive unconformity-bound units with different textural
330 features, sedimentary structures, and origins (a stratigraphic section is shown in
331 Supplementary Material).

332

333 The lower unit ranges from 10 to 20 m in thickness. It consists of chaotic, poorly
334 to extremely poorly sorted, matrix-supported, boulder-to-pebble-sized breccias. The
335 clasts mainly consist of basaltic dikes and lavas, although there are also fragments of
336 gabbros and pyroxenites. They are angular to subangular, up to 2 m size, and they do
337 not show any preferential orientation. The matrix is a mixture of sand and fine pebble-
338 sized particles with the same composition as the clasts. The unit has a massive
339 appearance, although a crude inverse grading can be observed at the base. A large
340 stratified block formed by a sequence of ropy basaltic lavas (roughly 50 m thick) and
341 scattered, metre-scale blocks with a jigsaw-fit structure are also present towards the
342 lower part of the unit. This unit represents the first stage of the slide scarp fill after its
343 lateral gravitational collapse.

344

345 The upper unit reaches some 100 m in thickness and displays a greater lateral
346 extension than the underlying one. The boundary between both is a sharp and irregular
347 erosive surface. The bulk of this unit is made of moderately-to-poorly sorted, slightly

bouldery, pebble-to-cobble clast-supported conglomerates in decimetre- to-metre scale beds, which are crudely interstratified with fine-to-medium pebble gravel and subordinate coarse pebbly sandstones. The clasts vary from subangular to rounded and mainly lie parallel to the bedding, although an a-axis imbrication of the elongate clasts is also present. The bed geometries vary from irregular to lenticular, with sharp and slightly erosive bases, to laterally continuous at outcrop scale. Planar and trough medium-scale cross-strata are commonly visible throughout the unit in the pebble and sandstone intervals. Coarse boulders are found widely dispersed as outsized clasts or concentrated in scours that may reach 1 m in depth. Some beds also display a reverse-to-normal grading. Large-scale planar cross-bedding with inclined laminae displaying a sigmoid shape present at the lower part of the unit is thought to represent frontal or lateral accretion units of macroforms within alluvial channels. There are frequent interbedded basaltic lavas.

DISCUSSION

Interpretation of the structures observed: the slide surface of the Tazo landslide

The major contact defined in the structural description systematically separates the volcanic breccias infilling the Tazo slide amphitheatre at its top, and variably deformed rocks of the Basal Complex and Lower Old Edifice at its base. A deformation gradient can be observed below the contact surface, with the most intensely deformed rocks located immediately below and along that surface. These features, together with the large spatial continuity of the contact surface across the area studied (Fig. 2), lead us to propose that it would correspond to the main slip surface of the Tazo slide. In some sectors of the Tazo slide (Points 5 and 6), the base of the volcanic breccia is formed by

374 an ultrafine-grained gouge, which forms a band of around 2 cm in thickness. NW-
375 oriented striae are observed locally in this band, indicating the slip direction. The
376 microscopic characteristics of this gouge suggest that the survivor grains can be treated
377 as rigid clasts in a viscous flow. A gravitational flank landslide of a volcanic edifice can
378 be considered a low-angle normal fault in which the footwall remains immobile and the
379 hanging wall moves along the fault plane, either as a single block (translational sliding)
380 or as a block that becomes disintegrated during its movement due to the progressive
381 fracturing, disaggregation, and mixing that occur during the flow, leading to the
382 formation of a rock slide debris avalanche. Thus, as in a normal fault, the elements of
383 the footwall exhibit deformation due to the relative movement of the hanging wall.
384 Indeed, in the gravitational landslide of Tazo, the underlying rocks below the slip
385 surface underwent a significant degree of deformation: the folding of lava flows and
386 dikes due to the dragging effect of the sliding block, the fracturing of lava flows,
387 plutonic rocks and dikes whose fragments form bands parallel to the movement surface,
388 giving rise to fault breccias and gouges, and the opening of cracks perpendicular to the
389 movement of the hanging wall. The cracks infilled by cemented breccias are typically
390 oriented perpendicular to the slide surface (Fig. 5A, compare “slide surface” and
391 “clastic dikes”) and to the slide direction at each point, and they always appear close to
392 the main slide surface. They are therefore interpreted as clastic dikes associated with
393 motion along the main slide surface.
394
395 The characteristics of the deformation associated with the Tazo landslide (the
396 formation of low cohesion fault rocks, fault breccias and gouges) indicate strong, brittle
397 deformation conditions at very high structural levels at depths lower than 4 km (Twiss
398 and Moores 1992). As seen previously, the deformation has affected both the materials

399 belonging to the Lower Old Edifice (pahoehoe flows, sills and dikes) and the rocks of
400 the Basal Complex (gabbros, pyroxenites, submarine volcanic rocks, and dikes), whose
401 different fabrics and mechanical behaviour gave rise to contrasting structures.
402
403 In the case of the lava flows, dikes, and sills of the Lower Old Edifice, the
404 generation of fault breccias and granular gouges would essentially have been related to
405 the cataclastic flow (Blenkinsop 2000). In the case of the rocks of the Basal Complex,
406 the deformation associated with the landslide in the footwall is indicated by the
407 formation of an incipient fracture cleavage, marked by the presence of numerous small
408 faults in the damaged zone. It is very possible that the presence of metamorphic
409 minerals (actinolite, chlorite, epidote, albite) arising from the hydrothermal greenschist
410 metamorphism shown by the rocks of the Basal Complex would have conditioned the
411 different pattern of deformation of these rocks, as compared with the unaltered lavas,
412 dikes, and sills of the Lower Old Edifice. The transformation of disaggregated host
413 rocks into assemblages of breccia, and then gouge, records the progressive increase in
414 the total shear strain imposed by the cumulative slip of the landslide. Additionally, the
415 mobilization of the granular gouge that fills small cracks as clastic dikes cutting across
416 the slip plane and intruding the overlying volcanic-breccia deposits (Fig. 6B) suggests
417 the presence of high pore-fluid pressures within the landslide surface (Day, 1996). The
418 deformation of the footwall would have been coeval with the landslide process,
419 although it probably lasted for an undetermined period of time prior to the catastrophic
420 event. During that period, the rocks were gradually deformed in a process similar to
421 creep. After the yield strength had been attained, the sudden gravitational collapse of a
422 large portion of the edifice occurred.
423

The mechanism of gouge formation was probably frictional shearing owing to the emplacement of the overlying cohesive debris flow or debris avalanche. The presence of frictional gouge at the base of volcanic or non-volcanic landslide deposits ("frictionites") or slumps has been reported worldwide. For instance, in the San Andrés fault, on the island of El Hierro (Canary Islands), which is interpreted as having been produced by an aborted sliding (Day et al. 1997), there are cataclasites formed at shallow depths, attributed to large displacements along the fault during a single event. Fine-grained layers at the base of debris-avalanche deposits showing shearing features have been reported for other volcanic locations, such as the debris-avalanche of the Chimborazo sector collapse, in Ecuador, Bernard et al. (2008). Schneider and Fisher (1998) found a zone of strongly foliated gouge at the base of a debris avalanche related to the collapse of the north-western flank of the Cantal Volcano. This foliated gouge overlies a Variscan leucogranite. The gouge fills open cracks in the underlying leucogranite, forming clastic dikes. Those authors concluded that the formation of the gouge and the opening of cracks in the leucogranitic basement were contemporaneous, and that the frictional shearing due to the emplacement of the debris avalanche generated the gouge. On Réunion Island, the lava flows located under the Saint-Gilles breccias that represent debris-avalanche deposits produced by the slide of the western flank of the Piton des Neiges exhibit an intense striation and cataclasis due to the friction and rubbing of the slid mass over the upper surface of the lava flows (Bachèlery et al. 2003). Those authors described the appearance of frictional surfaces at the contacts between the diverse rocky avalanche breccia levels that make up the "Saint Gilles breccias" unit on Réunion Island. They are characterized by shearing bands and fine-grained cataclasites produced by the deceleration affecting the slid masses when they passed over topographical irregularities (indicated by a change in the slope angle)

449 on the shore of the island. Similar characteristics have been observed in non-volcanic
450 slides. The study of giant submarine landslides has revealed the presence of erosional
451 slide scars, striations on the basal sliding surface, and landslide blocks within a chaotic
452 debris-flow matrix (e.g. Gee et al. 2006). Transitions from rock- and debris-avalanches
453 to distal debris flows have been described in large continental landslides associated with
454 excessive rainfall periods in mountainous areas (Shang et al. 2003). The friction-related
455 gouge recognized at the base of the volcanic breccia above the slip plane of the
456 landslide of Tazo suggests an *en masse* emplacement. Consequently, deposition would
457 have occurred when the debris avalanche or the cohesive debris flow behaved as a rigid
458 sliding mass. Friction probably acted during the last stages of transport, because friction
459 leads to a rapid slowing down and arrest of the debris avalanche or the cohesive debris
460 flow. Before complete arrest of the granular mass, the debris avalanche or the cohesive
461 debris flow would have had to change from a non-turbulent fluidized state into a rigid
462 solid state. This rheological transformation probably occurred very quickly, as
463 suggested by Schneider and Fisher 1998.
464
465 The kinematic data reported here provide further information about the sliding
466 process. At many of the points studied, the kinematic criteria point to an ENE-WSW-
467 trending displacement and extension (Fig. 5, 7). The structures associated with this
468 direction of extension will be referred as Set 1, and include the folds at Point 2 (Fig.
469 5A), the small faults at Point 4, the folded dikes, faults, and slickenside striations
470 observed on the slide surface at Point 5 (Fig. 7A), and the older striations on the slide
471 surface at Point 6 (Fig. 7B). However, for an explanation of the large-scale geometry of
472 this slide a NNW-SSE collapse would be required (Fig. 2, 8). In fact, the axis of the
473 curved, concave-upwards sliding surface is NNW-SSE-trending and plunges slightly to

474 the NNW (Fig. 9A). Indeed, some local structures strongly suggest late N-S to NNW-
475 SSE displacements, such as the clastic dikes at Point 2 (Fig. 5A, B), the late faults at
476 Point 4 (Fig. 5C), and the younger striation on the sliding surface at Point 6 (Fig. 7B).
477 These younger structures will be referred to as Set 2. The field data also suggest that
478 both sets of structures developed within a short interval of time from each other. For
479 example, the clastic dikes are almost perpendicular to the axes of the previous folds.
480 Although the structures of Set 2 are usually later than those of Set 1, more complex
481 cross-cut relationships are observed locally, with faults indicating NNW extension
482 displaced by the faults of Set 1 and, again, both generations of structures affected by the
483 faults of Set 2. Rotation of the blocks also produced local features, such as rotated low-
484 angle normal faults, currently with an apparently reverse displacement, and true reverse
485 faults, probably due to stress heterogeneities or to local buttressing effects (Fig. 5C). All
486 these data are coalesced in Fig. 9B and 9C. The blue and red arrows indicate the old
487 (Set 1) and more recent (Set 2) displacements, respectively. How should this pattern of
488 two, almost normal displacement fields be interpreted, and how should it be reconciled
489 with the evolution of a large volcano flank slide such as the Tazo collapse? A possible
490 analogue can be observed in the tectonic evolution of the island of Stromboli. There, the
491 local extension direction became reoriented in the footwall of the large slide from a
492 regional NW-SE trend towards a radial pattern, perpendicular to the limits of the
493 unbuttressed depression of the sector collapse (Tibaldi 1996). Another factor that would
494 have favoured this extension perpendicular to the slide boundary is the rollover of the
495 upper surface of the spreading block and its substratum. The ENE-WSW extension
496 direction (blue arrows, Fig. 9) and associated faults may have been a response to the
497 large-scale folding of the displaced block. The structures of Set 2 (red arrows in Fig. 9)
498 reflect the large-scale displacement trajectories associated with the collapse. Similar

trajectories have been obtained in analogous models of volcanoes spreading above tilted substrata (Wooller et al. 2004) or of flank-collapse in weak-cored volcanoes (Cecchi et al. 2005). Although the large-scale folding and collapse of the hanging wall were essentially contemporaneous processes (actually, the folding process is a result of the displacement of the hanging wall block above its curved basal surface), we believe that most of the deformation related to the folding took place early on during the collapse. A detailed structural analysis of zones similar to the Tazo slide would be necessary to better understand the physical process of the gravitational collapse of large volcanoes.

Interpretation of the deposits filling the amphitheatre formed by the Tazo landslide and their significance in the context of the Canary Islands.

The rocks infilling the scar of the Tazo landslide are composed of two successive unconformity-bound units with different textural features, sedimentary structures, and origins.

The sedimentological features of the lower unit, located above the slide surface, suggest that both deposits were formed by a cohesive debris (a matrix-supported deposit of massive character) and by a debris-avalanche (megablocks up to 15 m in size, jigsaw-fit textures). In this sense, the existence of megablocks and jigsaw-fit textures suggests that the lower unit could have been the result of a cohesive debris-flow deposit that was produced by the transformation of the distal portion of a water-saturated debris avalanche during its transport (Capra et al. 2002). Alternatively, it is possible that the slide of the flank of the edifice gave rise to a cohesive debris flow directly. In that case, the jigsaw-puzzle texture would have been formed during the initial dilation of the rock

524 at the time of the collapse, and not by the granular collisions during flow, as suggested
525 for Mount St Helens (Glicken, 1998). These primary structures may be preserved in the
526 upper portion of the debris-flow deposit. A flank collapse affecting an edifice after an
527 intense hydrothermal alteration (clay-rich), with high water contents (an edifice with an
528 important aquifer), could generate such a cohesive debris flow (Capra and Macías 2000;
529 Capra and Macías 2002; Capra et al. 2002), although at Mombacho it did not (Van Wyk
530 deVries and Francis 1997). The presence of jigsaw-puzzle textures is not exclusive of
531 debris-avalanche deposits; they may also be found in cohesive debris flows coming
532 from the transformation of a debris avalanche (Capra and Macías 2002). The occurrence
533 of an inversely graded layer at the base of the deposit suggests that the flow developed a
534 dilute basal layer, in which the main clast-supporting mechanism was dispersive
535 pressure. This feature is consistent with the hypothesis that mechanical fluidization
536 would have acted as a possible dispersive process for the particles in a large-scale
537 granular flow (Schneider and Fisher 1998).
538
539 Concerning the offshore extension of these deposits, Acosta et al. (2005) and the
540 Instituto Español de Oceanografía (2006) have identified several lobes of debris-
541 avalanche deposits located in the north and north-western part of La Gomera, on the
542 ocean floor. The westernmost lobes could correspond to the currently-submerged
543 deposit of the Tazo gravitational landslide (Fig. 8).
544
545 The upper unit represents a second stage in the filling of the slide scar, and it
546 contains features attributable both to sediment-charged, high-energy and poorly
547 confined water-laid sheetfloods and hyperconcentrated flows. The scattered cobbles and
548 boulders may represent rock-fall processes (Lirer et al. 2001). This second unit would

549 almost certainly have been formed by the re-sedimentation of the debris-avalanche
550 material formed by the landslide and by the collapse and erosion of the amphitheatre
551 walls.
552
553 On the island of Tenerife, in the subsurface of some valleys, such as the Orotava,
554 Güímar or Icod valleys, there are sedimentary deposits buried under hundreds of metres
555 of lava flows that fill ancient paleo-amphitheatres formed by gravitational flank
556 landslides (Bravo 1962; Navarro and Coello 1989; Ancochea et al. 1999). These
557 deposits have been termed "mortalón" (a name given by the people who worked at the
558 many galleries for groundwater exploitation), and consist of chaotic clastic
559 agglomerates composed of rock fragments of all sizes, up to several tons in weight (
560 (the "fanglomerado" of Bravo, 1962) enclosed in a clayey sandy matrix, of laminated
561 clayey-silty deposits of lacustrine origin, and also of conglomerates and breccias
562 originated by debris flow, hyperconcentrated flows, sheetfloods and talus deposits. All
563 these deposits (the so-called "mortalones") have often been interpreted as debris
564 avalanches originated by the gravitational landslides that eroded these valleys (Navarro
565 and Coello 1989). These deposits are sometimes hundreds of metres thick (Bravo 1962;
566 Navarro and Coello 1989; Márquez et al. 2008a; Márquez et al. 2008b). However, as
567 shown here most of them are not necessarily debris-avalanche deposits; instead, they
568 could be debris flows, hyperconcentrated flows, sheetfloods, or talus and lacustrine
569 deposits.
570
571 The two-episode process of filling the scar formed by the gravitational landslide
572 at Tazo could serve as a model to explain the formation of the above mentioned
573 "mortalón"-type deposits, as has been proposed at other similar landslide amphitheatre

574 infills in the Canary Islands (Playa de La Veta and Cumbre Nueva in La Palma,
575 Colmenero et al. 2008; Teno and at Anaga at Tenerife, Walter et al. 2005, Walter and
576 Schmincke 2002) and in other geodynamic contexts, such as at the Cantal volcano in
577 France (Reubi and Hernandez 2000; Nehlig et al. 2001; Arnaud et al**.** 2002) and Etna in
578 Italy (Calvari et al. 1998).
579
580 **Causes of the slide**
581
582 Many causes have been proposed to explain the destabilization of large volcanic
583 edifices on Earth, such as those listed by McGuire (1996). These causes are associated
584 with the activity of the volcanoes themselves. They include the intrusion of dikes and
585 sills, the intrusion of cryptodomes or plutonic bodies, the overweight related to the
586 accumulation of volcanic products, phreatic eruptions, vertical collapse related to
587 magma withdrawal in shallow magmatic chambers, seismic activity, and increases in
588 fluid pressure. Factors related to the structure of the edifice itself may also be of
589 relevance, including the presence of hydrothermal alteration zones, olivine cumulates,
590 hydroclastic materials, volcanoclastic, pyroclastic or argillaceous paleosol levels and
591 clayey layers. Finally, the influence of other factors such as gravitational spreading,
592 changes in sea level, or the reactivation of faults in the substrate must also be taken into
593 consideration.
594
595 In old landslides it is difficult to know the internal or external causes that
596 triggered the destabilization of the volcanic edifices with any degree of accuracy.
597 Regarding the Old Edifice of La Gomera, the geological data are indicative of a
598 conventional shield volcano (Ancochea et al. 2006). This edifice could have had a

599 diameter of around 22 km (Ancochea et al., 2006). The centre of the original
600 construction would have been situated in the vicinity of Vallehermoso, some 8 km north
601 of the central zone of the present island (Ancochea et al. 2008). The northern rim of the
602 emergent edifice probably extended for about 5 km offshore from the present northern
603 coastline. This accounts for the shallower and less steep sea floor observed in this area.
604 A volcanic edifice of such dimensions, if slopes dipping from 7° to 10° are assumed,
605 may have reached an altitude of 1300 to 1900 m (Ancochea et al. 2006). This edifice
606 underwent important landslides towards the NW and the NE, which would explain why
607 a large part of its northern flank is currently below sea level (Ancochea et al. 2006).
608
609 The slip plane affected very diverse materials with very different mechanical
610 characteristics, ranging from the pahoehoe lavas, sills, and vertical dikes of the Lower
611 Old Edifice, to the submarine volcanic and plutonic rocks of the Basal Complex,
612 intruded by an important dike swarm. The mineralogy of the greenschist facies rocks of
613 the Basal Complex must have diminished their mechanical resistance, facilitating their
614 deformation. Cecchi et al. (2005) have described the flank spreading and collapse of
615 volcanoes with hydrothermally weakened cores, and their predicted deformation field
616 coincides with that corresponding to Set 2 of the structures at the Tazo landslide.
617 Therefore, it is suggested that the Tazo landslide can be considered an example of flank
618 spreading favoured by hydrothermal alteration at the core and base of the edifice, a
619 process so far described for only a few volcanoes (e.g. Casita volcano, Nicaragua, van
620 Wyk de Vries et al. 2000).
621
622 The orientation and abundance of the dikes that intruded the rocks of the Basal
623 Complex seem to outline a rift zone in the northern sector of the island that would have

624 been active during the first stages of the formation of the Lower Old Edifice. This rift
625 zone, oriented ENE-WSW, is clearly perpendicular to the slip direction of the Tazo
626 landslide (Fig. 8). On oceanic islands**,** landslides usually occur on the flanks of rift
627 zones (the landslide is oriented perpendicular to a single dominant dike zone) or at the
628 junction of two rifts with different orientations (the sector collapse bisects the angles
629 formed by two intersecting zones of persistent diking (McGuire 1996). The repeated
630 intrusion of magma into the rift axis could have triggered the Tazo gravitational slide.
631 Additionally, it is necessary to highlight the existence of important ENE-WSW-oriented
632 tectonic features in this northern sector of the island affecting the Basal Complex
633 (Casillas et al. 2008), such as the normal faults of the Montaña de Alcalá and Guillama
634 (Fig. 1). The ENE-WSW strike of these faults indicates a regional structural trend in the
635 Canary Islands Archipelago. Using seismic and gravimetric methods, Dash and
636 Bosshard (1969) detected a major fracture line that is consistent in orientation and
637 location with those faults and that extends from El Hierro throughout the northern part
638 of La Gomera up to the Teno and Anaga Massifs, both of them in northern Tenerife
639 (Fig. 8). It is very possible that the displacement associated with these regional normal
640 faults could have downthrown the northern part of La Gomera to a considerable extent
641 in a NNW-SSE direction, this being the main cause of the destabilization of this sector
642 of the Lower Old Edifice. Interestingly, the NNW-SSE-directed displacement shown by
643 both regional faults coincides with the collapse direction of the Tazo landslide. This
644 destabilization mechanism was tested experimentally by Vidal and Merle (2000), and
645 later documented by Merle et al (2006) for the island of Nuku Hiva (Marquesas
646 Archipaelago), considering volcanic edifices of sizes similar to that of the Lower Old
647 Edifice affected by the activity of normal faults. The analogous models of dip-slip faults
648 positioned below the flanks of heterogeneously layered cones (Wooler et al. 2009),

649 which exactly coincide with the location of the Guillama and Montaña de Alcalá faults
650 with respect to the Lower Old Edifice (Figs. 1 and 8), predict the generation of a large-
651 scale instability and collapse perpendicular to the fault strike, in complete agreement
652 with the characteristics of the Tazo landslide.
653
654 **CONCLUSIONS.**
655
656 The Old Edifice of La Gomera underwent a large landslide on its north-western
657 flank. The rocks underlying the slip plane have abundant deformation features. Thus,
658 the lava flows and the dikes of the Lower Old Edifice are folded and intensely crushed,
659 and the slip plane is indicated by the existence of a foliated fault breccia and a foliated
660 granular gouge. Also, where the slip plane affects the rocks of the Basal Complex the
661 dikes are also folded, and the gabbros and pyroxenites are affected by small but
662 numerous faults, which have given rise to the formation of an incipient fracture
663 cleavage. In this case, the slip plane is indicated by the presence of foliated fault
664 breccias and foliated gouges. The slip plane is overlain by a debris avalanche or
665 cohesive debris-flow deposit, the base of which is characterized by the presence of a
666 striated, ultra-fine gouge formed as a consequence of frictional shearing due to the
667 emplacement of the debris avalanche or cohesive debris-flow.
668
669 The kinematics of the landslide includes a first stage of extension predominantly
670 perpendicular to the margins of the displaced block, interpreted in the footwall of the
671 sliding mass as being due to a reorientation of the regional deformation field near the
672 border of the newly generated unbuttressed depression. This stage partly coincided in
673 time with the extension parallel to the NNW-directed displacement of the hanging wall
674 block, which generated the dominant deformation field during the last stages of the

675 evolution of the landslide.

676

677 This important landslide may be related to the continuous injection of magma,
678 associated with the emplacement of dikes in an ENE-WSW-oriented rift zone, and/or to
679 the displacement associated with the activity of the normal faults of Guillama and
680 Montaña de Alcalá affecting the substratum of the Lower Old Edifice. The low
681 mechanical resistance of the rocks of the Basal Complex, to a large degree affected by a
682 hydrothermal metamorphism under greenschist facies conditions, also facilitated the
683 gravitational collapse of the overlying volcanic edifice.

684

685 The filling of the amphitheatre formed by the Tazo landslide occurred in two
686 stages. During the first stage, the materials generated directly by the flank gravitational
687 slide were deposited as a cohesive debris flow or as the product of the flow
688 transformation of the distal portion of a water-saturated debris avalanche. During the
689 second stage, and as a consequence of the re-sedimentation of the former deposits or as
690 a result of the erosion and collapse of the walls of the landslide scars, breccias and
691 conglomerates were deposited by debris flows, hyperconcentrated flows, sheetfloods
692 and talus deposit processes. This model of two filling stages of landslide scars can be
693 extrapolated to other landslides that have occurred in the Canary Islands and to other
694 places in the world, and it provides an alternative to the sedimentary deposits found in
695 the subsurface of Tenerife, popularly known as “mortalón”.

696

697

698 **ACKNOWLEDGEMENTS.**

699

Financial support from projects BTE 2003-00569, CGL 2006-00970/BTE and CGL2009-07775 of the Spanish Ministry of Education and Science and the Spanish Ministry of Science and Innovation and 2003/106 of the Canary Islands Regional Government is gratefully acknowledged. The original manuscript benefited from very careful reviews from Jean-Luc Schneider, Benjamin van Wyk de Vries, John Stix and an anonymous reviewer. We are indebted to Nick Skinner for his assistance with the English. The results described in this work were obtained within the framework of the activities of the Research Group "Submarine growth and emergence of the Canary Islands: a geologic study of the Basal Complexes" of the University of La Laguna. We thank Juan Coello Bravo for his comments about the exposures studied in La Gomera.

REFERENCES.

Abdel-Monem A, Walkins ND, Gast P (1971) Potassium-argon ages, volcanic stratigraphy and geomagnetic polarity history of the Canary Islands: Lanzarote, Fuerteventura, Gran Canaria and La Gomera. Am J Science 271:490-521

Acosta J, Uchupi E. Muñoz A, Herranz P, Palomo C, Ballesteros M, ZEE Working Group (2005) Geologic evolution of the Canarian Islands of Lanzarote, Fuerteventura, Gran Canaria and La Gomera and comparison of landslides at these islands with those at Tenerife, La Palma and El Hierro. Mar Geophys Res 24:1-40

Ancochea E, Huertas MJ, Cantagrel JM, Coello J, Fúster JM, Arnaud N, Ibarrola E

(1999) Evolution of the Cañadas edifice and its implications for the origin of the Cañadas Caldera (Tenerife, Canary Islands). J Volcanol Geotherm Res 88:177-1999

Ancochea E, Hernán F, Huertas MJ, Brändle JL, Herrera R (2006) A new chronostratigraphical and evolutionary model for La Gomera: Implications for the overall evolution of the Canarian Archipelago. J Volcanol Geotherm Res 157:271-293

Ancochea E, Brändle JL, Huertas MJ, Hernán F, Herrera, R (2008) Dike-swarms, key to the reconstruction of major volcanic edifices: The basic dikes of La Gomera (Canary Islands). J Volcanol Geotherm Res 173:207-216

Arnaud N, Leyrit H, Nehlig P, Binet F, Jamet A, Vannier W (2002) Les lahars du flanc nord-ouest du stratovolcan du Cantal. Géol Fr 1:3-13

Bachèlery P, Robineau B, Courteaud M, Savin C (2003) Debris avalanches on the western flank of Piton des Neiges shield volcano (Reunion Island). Bull Soc Géol Fr 174:125-140

Bernard B, van Wyk de Vries B, Barba D, Leyrit H, Robin C, Alcaraz S, Samaniego P (2008) The Chimborazo sector collapse and debris avalanche: deposit characteristics as evidence of emplacement mechanisms. J Volcanol Geotherm Res 176:36-43

751 Blenkinsop TG (2000) Deformation microstructures and mechanisms in minerals and
752 rocks. Kluwer, Dordrecht
753
754 Bravo T (1962) El circo de Las Cañadas y sus dependencias. Bol. R. Soc. Esp. Hist.
755 Nat. Secc. Geol. 60:93–108
756
757 Bravo T (1964) Estudio geológico y petrográfico de la Isla de La Gomera I: estudio
758 geológico. Estud Geol 20:1-21
759
760 Cantagrel JM, Cendrero A, Fúster JM, Ibarrola E, Jamond C (1984) K-Ar chronology of
761 the volcanic eruption in the Canarian Archipelago: Island of La Gomera. Bull
762 Volcanol 47:597-609
763
764 Calvari S, Tanner LH, Groppelli G (1998) Debris-avalanche deposits of the milo lahar
765 sequence and the opening of the Valle del Bove on Etna volcano (Italy) J
766 Volcanol Geotherm Res 87:193-209
767
768 Capra L, Macías JL (2000) Pleistocene cohesive debris fows at Nevado de Toluca
769 Volcano, central Mexico. J Volcanol Geotherm Res 102:149-168
770
771 Capra L, Macías, JL (2002) The cohesive Naranjo debris-flow deposit (10 km3): A dam
772 breakout flow derived from the Pleistocene debris-avalanche deposit of Nevado
773 de Colima Volcano (Mexico). J Volcanol Geotherm Res 117:213-235
774
775 Capra L, Macías JL, Scott KM, Abrams MD, Garduño-Monroy VH (2002) Debris

776 avalanches and debris flows transformed from collapses in the Trans-Mexican
777 Volcanic Belt, Mexico - behavior, and implications for hazard assessment. J
778 Volcanol Geotherm Res 113:81-110
779
780 Casillas R, Fernández C, De la Nuez J, García Navarro E, Colmenero JR, Martín MC
781 (2008) Deformaciones asociadas al deslizamiento gravitacional de flanco del
782 Edificio Antiguo Inferior en Tazo (La Gomera). Geotemas, 10:1269-1272
783
784 Cecchi E, van Wyk de Vries B, Lavest JM (2005) Flank spreading and collapse of
785 weak-cored volcanoes. Bull Volcanol 67:72-91
786
787 Cendrero A (1971) Estudio geológico y petrológico del Complejo Basal de la Isla de La
788 Gomera (Islas Canarias). Estud Geol 27:3-73
789
790 Cladouhos TT (1999) Shape preferred orientations of survivor grains in fault gouge. J
791 Struct Geol 21:419-436
792
793 Colmenero JR, de la Nuez J, Casillas R, Castillo C (2008) Caracteres de los
794 conglomerados y brechas epiclásticos de La Palma (Islas Canarias) y su relación
795 con grandes deslizamientos y génesis de la Caldera de Taburiente. Geotemas 10:
796 123-126
797
798 Cueto L, Balcells R, Gómez-Saínz JA, Barrera JL, Pineda A, Klein E, Cerrato M, Ruiz
799 MT, Brändle JL (2004a) Mapa y memoria explicativa de la hoja de Hermigüa
800 (1097 III) del Mapa Geológico Nacional: Madrid, Instituto Geólogico y Minero de

España, scale 1:25.000, 1 sheet

Cueto L, Gómez-Saínz J A, Barrera J L, Pineda A, Balcells R, Cerrato, M, Klein E, Ruiz M T, Brändle J L (2004b) Mapa y memoria explicativa de la hoja de Agulo (1097 IV) del Mapa Geológico Nacional: Madrid, Instituto Geólogico y Minero de España, scale 1:25.000, 1 sheet

Dash BF, Bosshard E (1969) Seismic and gravity investigations around the western Canary Islands. Earth Planet. Sci Lett 7:169–177

Day SJ (1996) Hydrothermal pore fluid pressure and the stability of porous, permeable volcanoes. In: McGuire W J, Jones, A P and Neuberg, J (eds). Volcano Instability on the Earth and Terrestrial Planets. Geol Soc Lond Spec Pub 110, pp 77-93

Day SJ, Carracedo JC, Guillou H (1997) Age and geometry of an aborted rift flank collapse: the San Andres fault system, El Hierro, Canary Islands. Geol Mag 134:523-537

Démeny A, Casillas R, Hegner E, Vennemann TW, Nagy G, Sipos P (2010) Geochemical and H-O-Sr-Nd isotope evidence for magmatic processes and meteoric-water interactions in the basal complex of La Gomera, Canary Islands. Miner Petrol 98:181-195, doi: 10.1007/s00710-009-0071-4

Gee MJR, Gawthorpe RL, Friedmann SJ (2006) Triggering and evolution of a giant submarine landslide, offshore Angola, revealed by 3D seismic stratigraphy and

826 geomorphology. J Sediment Res 76:9-19
827
828 Glicken H (1998) Rockslide-debris avalanche of May 18, 1980, Mount St. Helens
829 Volcano, Washington. Bull Geol Surv Jpn 49:55–106
830
831 Herrera R (2008) Volcanoestratigrafía, composición y evolución de los edificios
832 volcánicos subaéreos de La Gomera. PhD Thesis, Universidad Complutense de
833 Madrid
834
835 Herrera R, Huertas MJ, Ancochea E (2008). Edades ^{40}Ar–^{39}Ar del Complejo Basal de la
836 isla de La Gomera. Geogaceta 44:7–10
837
838 Instituto Español de Oceanografía (2006) Mapa Topobatimétrico del Archipiélago
839 Canario. Instituto Español de Oceanografía
840
841 Lirer L, Vinci A, Alberico I, Gifuni T, Bellucci F, Petrosino P, Tinterri R (2001)
842 Occurrence of inter-eruption debris flow and hyperconcentrated flood-flow
843 deposits on Vesubio volcano, Italy. Sediment Geol 139:151-167
844
845 Mardia KV (1972) Statistics of directional data. Academic Press, London
846
847 Márquez A, López I, Herrera R, Martín-Gonzalez F, Izquierdo T, Carreño F (2008a).
848 Spreading and potential instability of Teide Volcano, Canary Islands. Geophys
849 Res Lett 35: L05305, doi:10.1029/2007GL032625
850

851 Márquez A, López I, Herrera R, Martín-González F, Izquierdo I, Carreño F (2008b)
852 Reconstrucción geológica tridimensional del basamento del volcán Teide bajo el
853 Valle de Icod y la Caldera de Las Cañadas (Tenerife, Islas Canarias). Geotemas
854 10:1305-1308
855
856 Marrett R, Allmendinger RW (1990) Kinematic analysis of fault-slip data. J Struct Geol
857 12:973-986
858
859 Mehl KW, Schmincke H-U (1999) Structure and emplacement of the Pliocene Roque
860 Nublo debris avalanche deposits, Gran Canaria, Spain. J Volcanol Geotherm Res
861 94:105–134
862
863 Merle O, Barde-Cabusson S, Maury R, Legendre C, Guille G, Blais S (2006) Volcano
864 core collapse triggered by regional faulting. J Volcanol Geotherm Res 158:269-
865 280
866
867 Miller MG (1996) Ductility in fault gouge from a normal fault system, Death Valley,
868 California: a mechanism for fault-zone strengthening and relevance to
869 paleoseismicity. Geology 24:603-660
870
871 McGuire WJ (1996) Volcano instability: a review of contemporary themes. In: McGuire
872 WJ, Jones AP, Neuberg J (eds) Volcano Instability on the Earth and Terrestrial
873 Planets. Geol Soc Lond Spec Pub 110, pp 1-23
874
875 Navarro JM, Coello J (1989) Depressions originated by landslide processes in Tenerife.

876 Meeting on Canarian Volcanism, Eur Sci Found, Strasbourg, France
877
878 Nehlig P, Leyrit H, Dardon A, Freour G, De Ggoër de Herve A, Huguet D, Thiéblemont
879 D (2001) Repeated growth and catastrophic destruction of the Cantal
880 stratovolcano (France). Bull Soc Géol Fr 172:295–308
881
882 Paris R, Guillou H, Carracedo JC, Pérez-Torrado FJ (2005) Volcanic and morphological
883 evolution of La Gomera (Canary Islands), based on new K-Ar ages and magnetic
884 stratigraphy: implications for oceanic island evolution. J Geol Soc Lond 162:501-
885 512
886
887 Ramsay JG, Huber MI, (1987) The techniques of modern Structural Geology. Volume
888 2: Folds and fractures. Academic Press, London
889
890 Reubi O, Hernandez J (2000) Volcanic debris avalanche deposits of the upper Maronne
891 valley (Cantal volcano, France): evidence for contrasted formation and transport
892 mechanisms. J Volcanol Geotherm Res 102:271-286
893
894 Roa K (2003) Nature and origin of toreva remnants and volcaniclastics from La Palma,
895 Canary Islands. J Volcanol Geotherm Res 125:191-214
896
897 Schneider J-L, Fisher RV (1998) Transport and emplacement mechanisms of large
898 volcanic debris avalanches: evidence from the northwest sector of Cantal
899 Volcano. J Volcanol Geotherm Res 83:141–165
900

Shang Y, Yang Z, Li L, Liu D, Liao Q, Wang Y (2003) A super-large landslide in Tibet in 2000: background, occurrence, disaster, and origin. Geomorphology 54:224-243

Tibaldi A (1996) Mutual influence of dyking and collapses at Stromboli volcano, Italy. In: McGuire WJ, Jones AP, Neuberg J (eds) Volcano Instability on the Earth and Other Planets. Geol Soc Lond Spec Pub 110, pp 55-63

Twiss R, Moores E (1992) Structural Geology. Freeman, New York

Van Wyk de Vries B, Francis PW (1997) Catastrophic collapse at stratovolcanoes induced by gradual volcano spreading. Nature 387:387-390. doi:10.1038/387387a0

Van Wyk de Vries B, Kerle N, Petley D (2000) A sector collapse forming at Casita volcano, Nicaragua. Geology 28:167-170

Vidal P, Merle O (2000) Reactivation of basement faults beneath volcanoes: a new model of flank collapse. J Volcanol Geotherm Res 99:9–26

Walter TR, Schmincke H-U (2002) Rifting, recurrent landsliding and Miocene structural reorganization on NW-Tenerife (Canary Islands). Int. J. Earth. Sci. 91:615–628

Walter TR, Troll VR, Cailleau B, Belousov A, Schmincke HU, Amelung F, Bogaard P

(2005) Rift zone reorganization through flank instability in ocean island volcanoes: an example from Tenerife, Canary Islands. Bull Volcanol 67:281–291

Wooller L, van Wyk de Vries B, Murray JB, Rymer H, Meyer S (2004) Volcano spreading controlled by dipping substrata. Geology 32:573-476

Wooler L, van Wyk de Vries B, Cecchi E, Rymer H (2009) Analogue models of the effect of long-term basement fault movement on volcanic edifices. Bull Volcanol 71:1111-1131

FIGURE CAPTIONS:

FIGURE 1. Geologic map of the northern sector of La Gomera. The map is based on data from Cueto et al. (2004a) and Cueto et al. (2004b), as modified by us. The inset shows the location of La Gomera in the Canary Archipelago and the area covered by map.

FIGURE 2. Detailed geologic map of the Tazo landslide. The map is based on data from Cueto et al. (2004a) and Cueto et al. (2004b), as modified by us. The inset shows the location of La Gomera in the Canary Archipelago and the area covered by map.

FIGURE 3. A) Aerial image (view from northwest) of the Tazo landslide. B) Interpreted photograph of the sliding surface of the Tazo landslide on the coastline at Point 1.

FIGURE 4. Deformation structures and rocks related to the displacement along the contact (slide) surface between the volcanic breccias and their substratum at the outcrop near the village of Cubaba (Point 2 in Fig. 2). A) Interpreted photograph of an E-W-oriented infilled crack (clastic dike). B) Interpreted photograph of a folded sill. C) Photograph of the fault breccias and fault granular gouges below the contact surface. D) Photograph of the volcanic breccia located above the contact surface.

FIGURE 5. A) Structural data relative to Point 2. Equal-area, lower-hemisphere projection of layering (S_o, lava flows of the Lower Old Edifice below the contact surface and the breccia above the contact surface), sills, infilled cracks (clastic dikes) and contact surface (sliding surface). The squares mark the location of the statistical

962 fold axes for the folded lava flows and sills (see main text for an explanation of the
963 methodology used to determine fold axes). The confidence level of the fold axis
964 determination is > 99% for the S_o of lava flows and in the range of 90-95% for sills. The
965 large black arrow indicates the rotation of the lava flows and dikes towards a position
966 parallel to the sliding surface. B) Sketch depicting the geometry of the deformation
967 structures associated with the contact surface at Point 2. C) Structural data measured at
968 Point 4 projected on equal-area, lower-hemisphere diagrams. Cyclographic projection of
969 the contact surface and of late reverse and normal faults. The large white arrows
970 indicate the sliding direction according to the fault-slip data (see Supplementary
971 Material). In all cases, (n) indicates the number of measured data.
972
973 FIGURE 6. Photographs of the structures associated with the landslide near Tazo
974 (Points 4, 5 and 6 in Fig. 2). A) Photograph of the foliated fault breccia and foliated
975 granular gouge below the contact (sliding) surface. Note the volcanic breccia above the
976 slip plane. B) Foliated gouge intruding the volcanic breccia along a fracture, forming a
977 clastic dike. C) Photograph of the contact surface at Point 5. Folded dikes, P fractures,
978 and Riedel R2 surfaces below the contact surface can be observed at this point. D)
979 Photograph of the striated ultra-fine gouge at the contact surface at Point 6.
980
981 FIGURE 7. A) Equal-area, lower-hemisphere plot of the structural data measured at
982 Point 5. Contact (sliding) surface with slickenside striations marking the sliding
983 direction, and attitude of lava flows of the submarine volcanic rocks (footwall of the
984 sliding surface). The large white arrows indicate the location of the principal extension
985 axis, according to the results of the PT method (see Supplementary Material). Also
986 shown is the cyclographic projection of folded dikes located at the footwall of the

contact surface with the location of the statistical fold axis. See main text for an explanation of the methodology used to determine fold axis. The confidence level of the fold axis determination is > 99%. The large black arrow highlights the progressive rotation of the dikes towards a position parallel to the contact surface. B) Equal-area, lower-hemisphere plots of the structural data measured at Point 6. Contact surface and faults located in the vicinity of the contact surface and sub-parallel to it. The faults show two generations of slickenside striations (old and new). The large white arrows indicate the location of the principal extension, according to the results of the PT method (see Supplementary Material).

FIGURE 8. Sketch showing the possible location, extension, and displacement of the Tazo landslide relative to the Guillama and Montaña de Alcalá faults, the dikes in the Basal Complex, and the geophysical lineament observed by Dash and Bosshard (1969). The estimated dimensions of the Lower Old Edifice were taken from Ancochea et al. (2006). The bathymetric data are from Acosta et al. (2005). The location of the debris-avalanche deposits offshore La Gomera is from Acosta et al. (2005) and the Instituto Español de Oceanografía (2006).

FIGURE 9. A) Cyclographic projection (equal-area, lower hemisphere) of the sliding surface measured across the entire area studied. The red-shaded area marks the approximate axis of the large-scale, curved sliding surface. The blue and red arrows indicate the sliding direction (or the principal extension axis) at each location for the first and second stages, respectively (see main text for an explanation). B) Spatial orientation of the principal extension axes (yellow and red arrows) for the two main stages identified after the structural analysis of the sliding surface, as indicated above.

1012 For a legend, see Fig. 2. See main text for an explanation. C) Sketch depicting the three-

1013 dimensional geometry of the Tazo slide.

1014

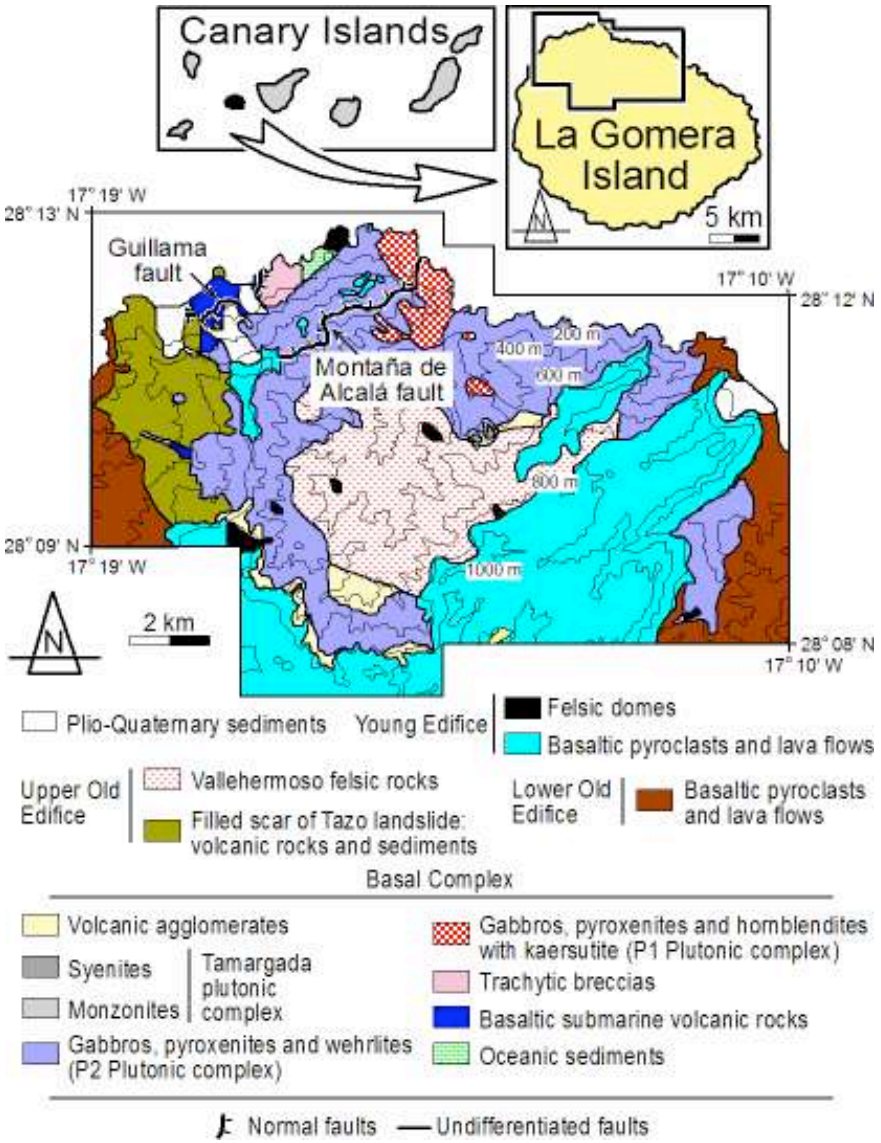
Canary Islands
La Gomera Island
5 km
17° 19' W
28° 13' N
Guillama fault
17° 10' W
28° 12' N
200 m
400 m
600 m
Montaña de Alcalá fault
800 m
1000 m
28° 09' N
17° 19' W
2 km
N
28° 08' N
17° 10' W
Plio-Quaternary sediments
Young Edifice
Felsic domes
Basaltic pyroclasts and lava flows
Upper Old Edifice
Vallehermoso felsic rocks
Filled scar of Tazo landslide: volcanic rocks and sediments
Lower Old Edifice
Basaltic pyroclasts and lava flows
Basal Complex
Volcanic agglomerates
Syenites
Monzonites
Tamargada plutonic complex
Gabbros, pyroxenites and wehrlites (P2 Plutonic complex)
Gabbros, pyroxenites and hornblendites with kaersutite (P1 Plutonic complex)
Trachytic breccias
Basaltic submarine volcanic rocks
Oceanic sediments
Normal faults
Undifferentiated faults

Fig. 1

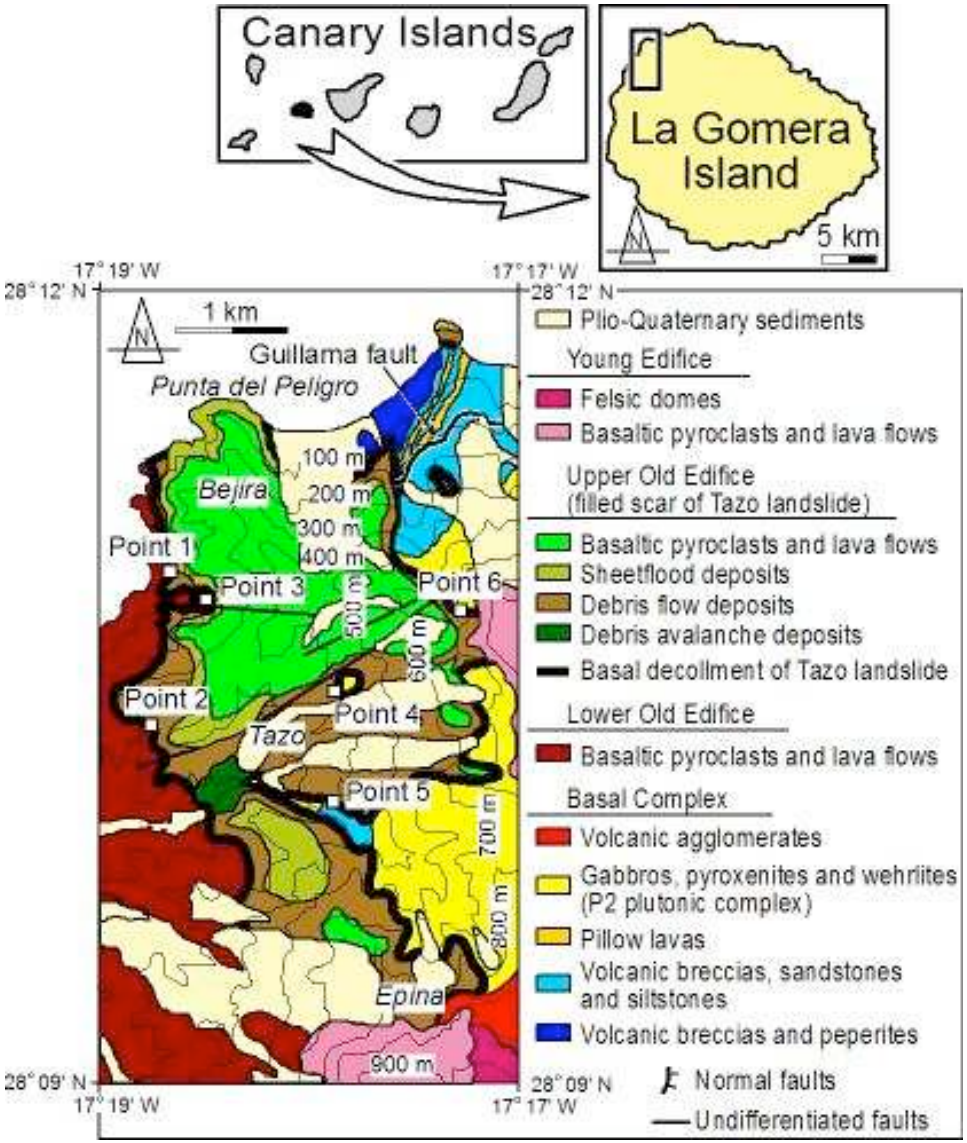
Canary Islands
La Gomera Island
5 km
17° 19' W
17° 17' W
28° 12' N
28° 09' N
1 km
Guillama fault
Punta del Peligro
Bejira
Point 1
Point 2
Point 3
Point 4
Point 5
Point 6
Tazo
Epina
100 m
200 m
300 m
400 m
500 m
600 m
700 m
800 m
900 m
Plio-Quaternary sediments
Young Edifice
Felsic domes
Basaltic pyroclasts and lava flows
Upper Old Edifice
(filled scar of Tazo landslide)
Basaltic pyroclasts and lava flows
Sheetflood deposits
Debris flow deposits
Debris avalanche deposits
Basal decollment of Tazo landslide
Lower Old Edifice
Basaltic pyroclasts and lava flows
Basal Complex
Volcanic agglomerates
Gabbros, pyroxenites and wehrlites
(P2 plutonic complex)
Pillow lavas
Volcanic breccias, sandstones
and siltstones
Volcanic breccias and peperites
Normal faults
Undifferentiated faults

Fig. 2

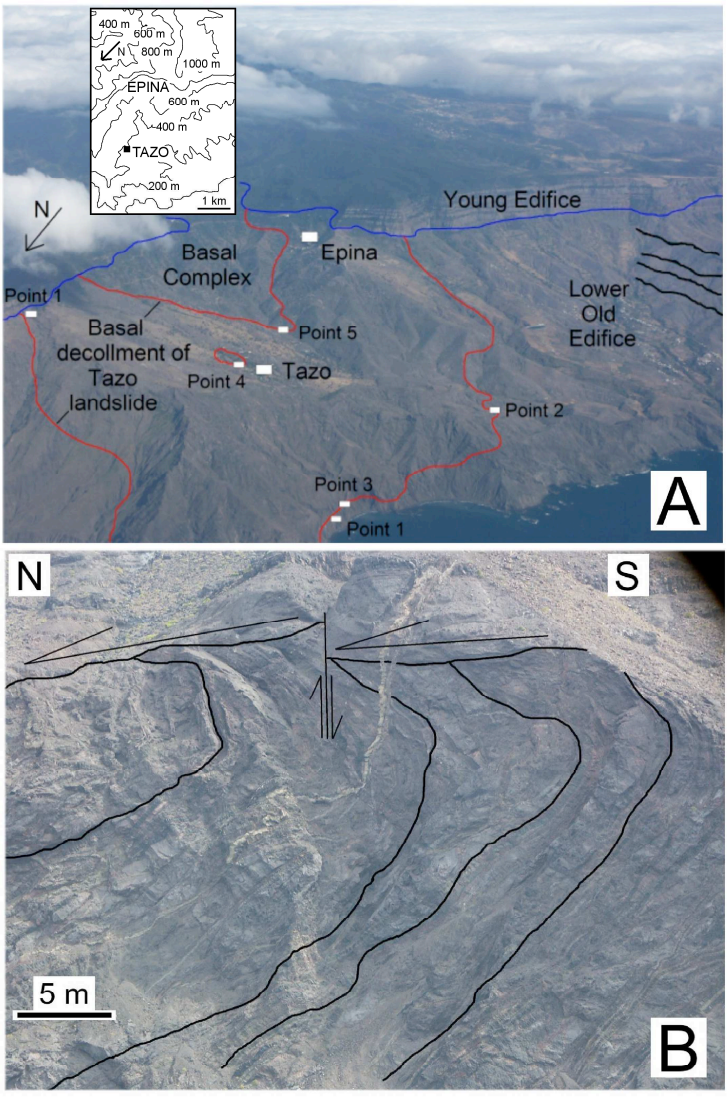
400 m
600 m
800 m
1000 m
N
EPINA
600 m
400 m
TAZO
200 m
1 km
N
Young Edifice
Basal
Complex
Epina
Point 1
Lower
Old
Edifice
Basal
decollment of
Tazo
landslide
Point 5
Point 4
Tazo
Point 2
Point 3
Point 1
A
N
S
5 m
B

Fig. 3.

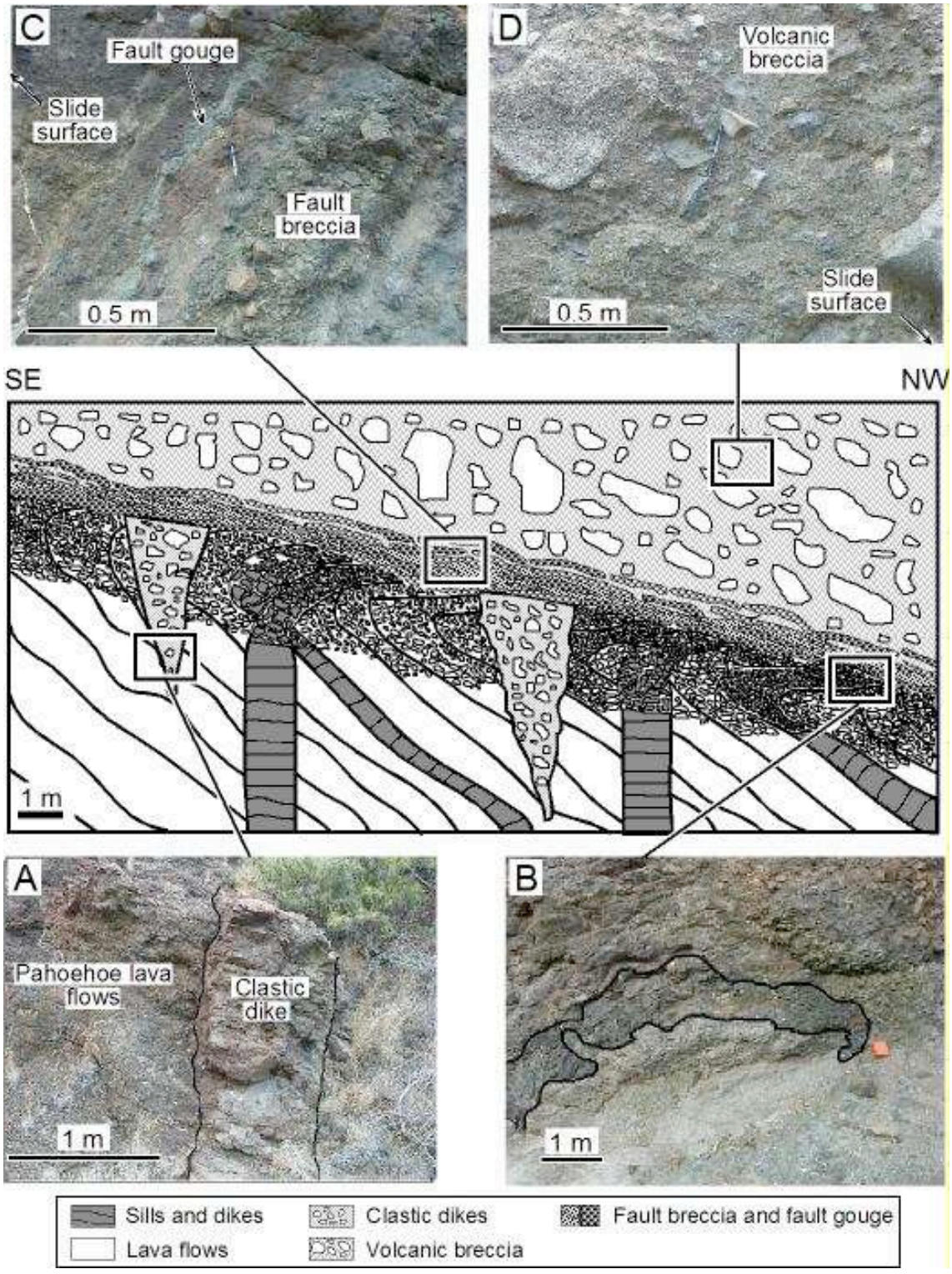
C
Fault gouge
Slide surface
Fault breccia
0.5 m
D
Volcanic breccia
Slide surface
0.5 m
SE
NW
1 m
A
Pahoehoe lava flows
Clastic dike
1 m
B
1 m
Sills and dikes
Lava flows
Clastic dikes
Volcanic breccia
Fault breccia and fault gouge

Fig. 4

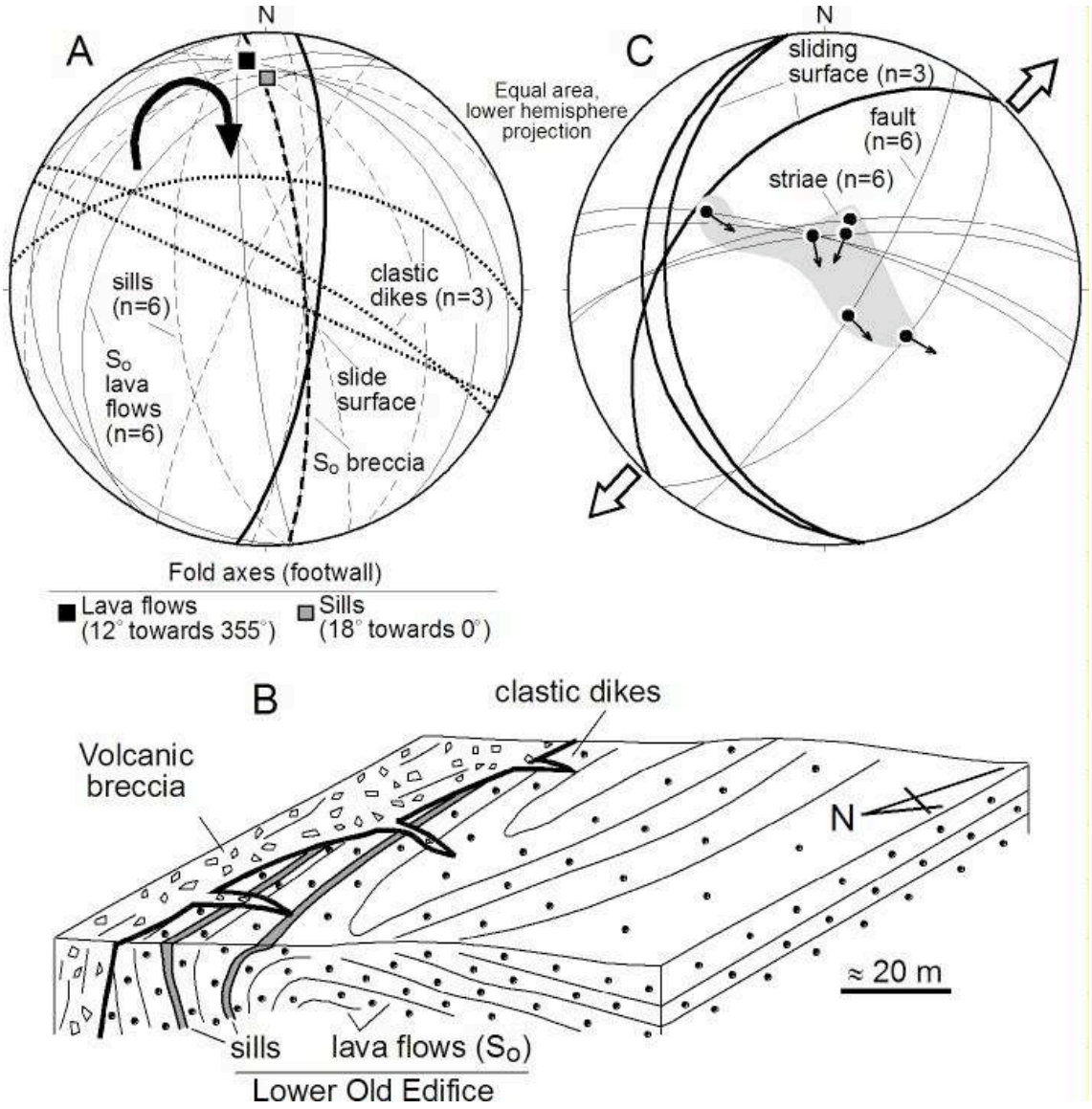
A
N
sills
(n=6)
So
lava
flows
(n=6)
clastic
dikes (n=3)
slide
surface
So breccia
Equal area,
lower hemisphere
projection
C
N
sliding
surface (n=3)
fault
(n=6)
striae (n=6)
Fold axes (footwall)
Lava flows
(12° towards 355°)
Sills
(18° towards 0°)
B
clastic dikes
Volcanic
breccia
N
≈ 20 m
sills
lava flows (So)
Lower Old Edifice

Fig. 5

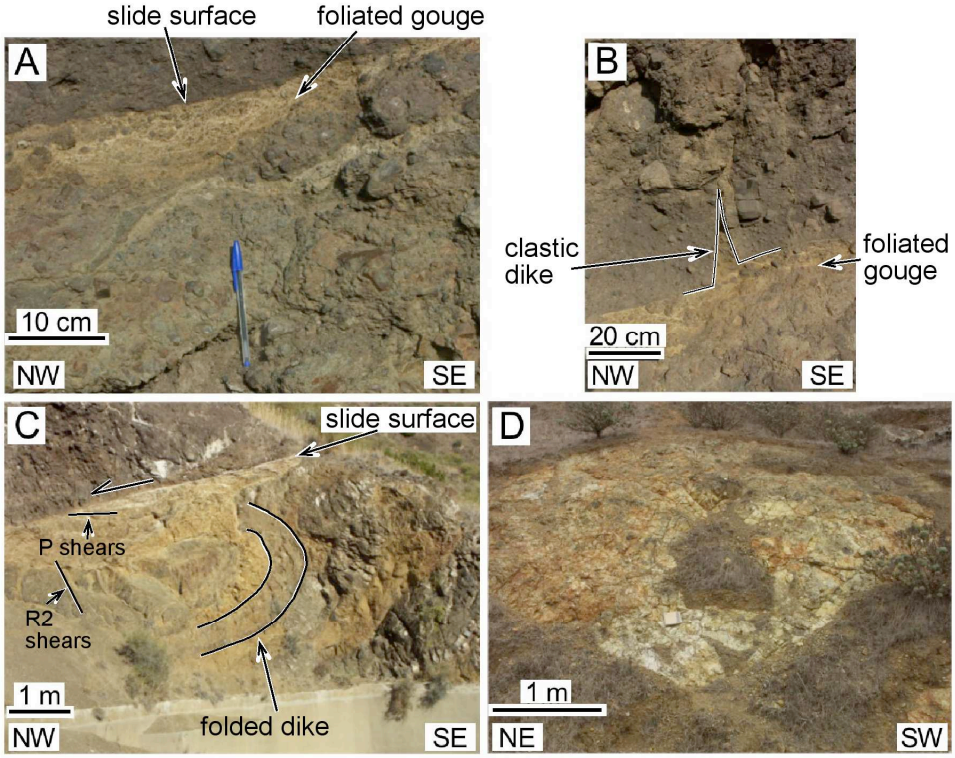
A
slide surface
foliated gouge
10 cm
NW
SE
B
clastic
dike
foliated
gouge
20 cm
NW
SE
C
slide surface
P shears
R2
shears
1 m
NW
folded dike
SE
D
1 m
NE
SW

Fig. 6

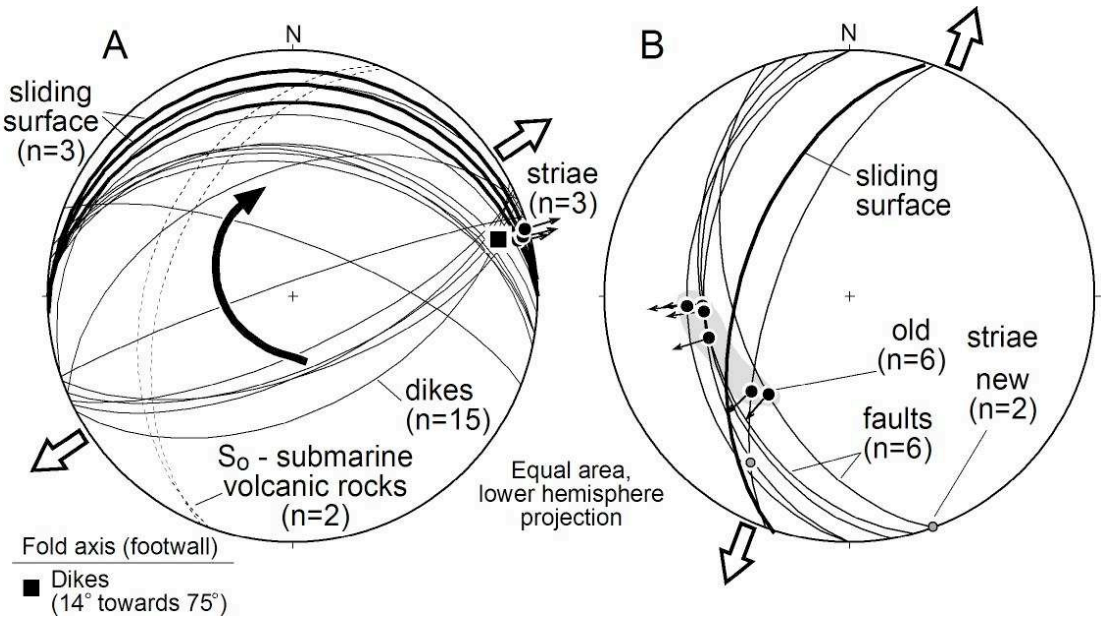
A
N
sliding
surface
(n=3)
striae
(n=3)
dikes
(n=15)
S_0 - submarine
volcanic rocks
(n=2)
Fold axis (footwall)
Dikes
(14° towards 75°)
Equal area,
lower hemisphere
projection
B
N
sliding
surface
old
(n=6)
striae
new
(n=2)
faults
(n=6)

Fig. 7

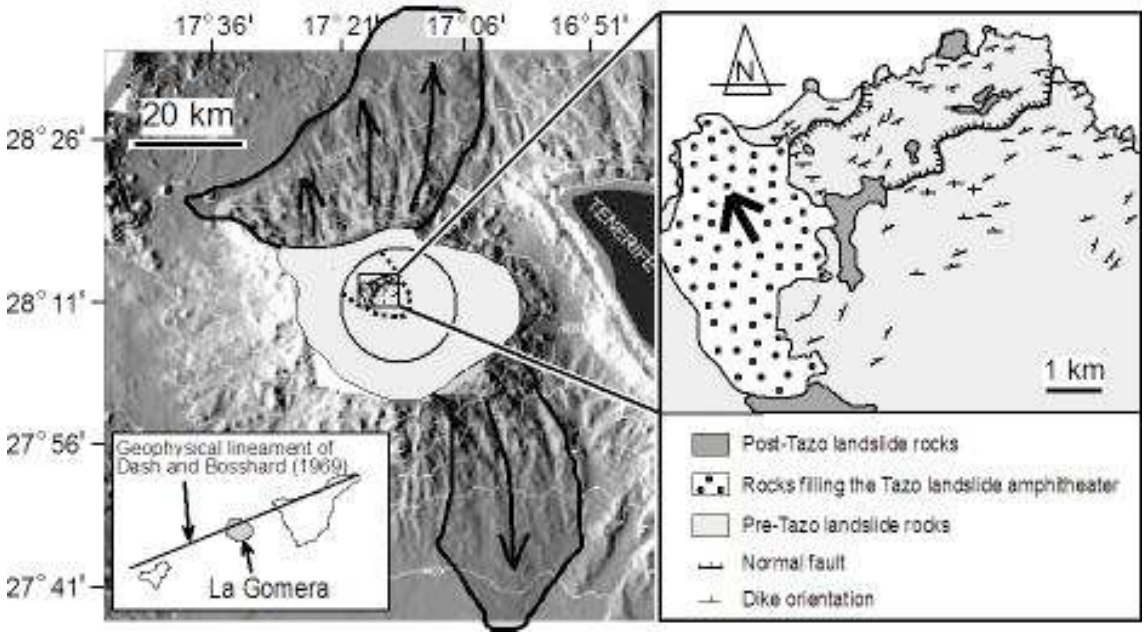
17° 36'
17° 21'
17° 06'
16° 51'
28° 26'
28° 11'
27° 56'
27° 41'
20 km
TENERIFE
Geophysical lineament of
Dash and Bosshard (1969)
La Gomera
N
1 km
Post-Tazo landslide rocks
Rocks filling the Tazo landslide amphitheater
Pre-Tazo landslide rocks
Normal fault
Dike orientation

Fig. 8

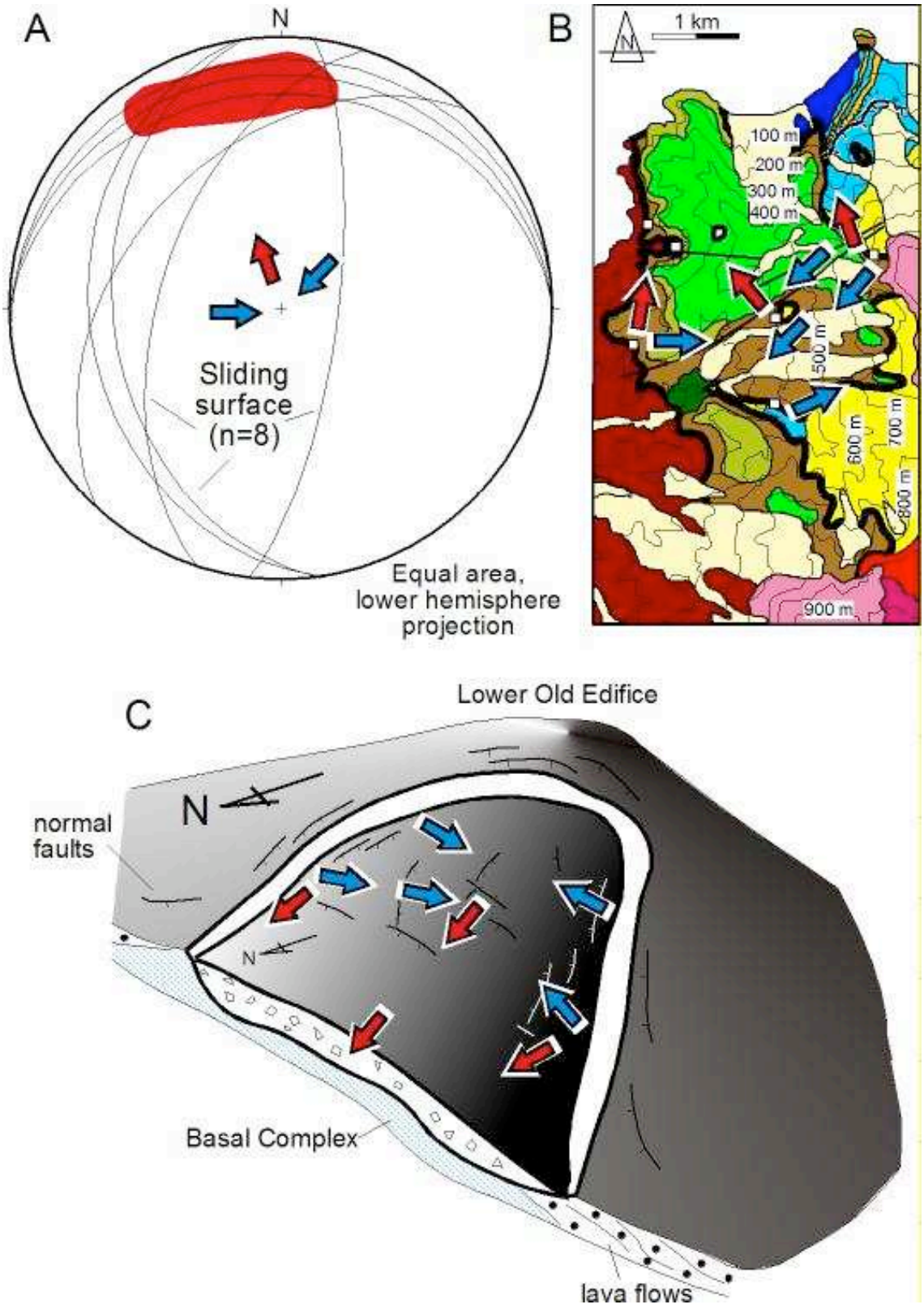
A
N
Sliding
surface
(n=8)
Equal area,
lower hemisphere
projection
B
N
1 km
100 m
200 m
300 m
400 m
500 m
600 m
700 m
800 m
900 m
C
Lower Old Edifice
N
normal
faults
N
Basal Complex
lava flows

Fig. 9